

The Feasibility of Au Ball Bonding on Sn-Plated Cu

J. LEE,^{1,2} M. MAYER,¹ and Y. ZHOU¹

1.—Microjoining Laboratory, Centre for Advanced Materials Joining, Department of Mechanical and Mechatronics Engineering, University of Waterloo, Waterloo, ON, Canada N2L 3G1
2.—e-mail: j75lee@engmail.uwaterloo.ca

The feasibility of thermosonic gold wire bonding on Cu coupons with Sn/Cu metallizations was studied by evaluating shear strength and microstructure of balls bonded on different Sn metallization samples. The $0.85 \pm 0.08 \mu\text{m}$ and $5.34 \pm 0.21 \mu\text{m}$ thick metallizations were produced by dipping the Cu coupon in 250°C molten Sn solder for 1 s (sample 1) and 30 s (sample 2), respectively. Cu_6Sn_5 intermetallic compounds are formed during dipping. After wire bonding, Au-Cu-Sn layers are found on the ball-coupon interface of both samples. The highest ball shear force observed was 40 gf (1 gf = 9.81 mN) and was achieved on sample 1 using 520 mW and 40 gf of ultrasonic power and bonding force, respectively. The shear fracture goes through the Au ball. The Sn is squeezed out of the contact zone during wire bonding and forms flashes that extend $5 \mu\text{m}$ and $25 \mu\text{m}$ beyond the contact zone for samples 1 and 2, respectively.

Key words: Thermosonic, wire bonding, tin, shear force, microstructure

INTRODUCTION

Wire bonding with ultrasound is one of the most commonly used processes in electronics packaging to electrically connect an integrated circuit with a lead frame or a substrate.¹ Current demands on miniaturization, high speed, and low power in electronics have led to thinner wire diameters and new materials for the wire and bond pads. Both the wire resistance and the wire-to-pad contact resistance should be reduced to increase switching speed of the integrated transistor.² A possible way is to replace the existing Al interconnects with metals of lower resistance.³ Thus, Cu metallizations are the industry's choice to satisfy the new requirement in terms of lower resistance, faster heat dissipation, higher current density, and higher speeds of ICs.

However, Cu oxidation and the high Cu hardness compared to Al are obstacles to be solved because they can result in nonbondable surfaces or can cause cracks in the chip during bonding.⁴ Harman et al.⁵ used thin inorganic films such as SiN, SiO₂, and Al₂O₃ deposited over the Cu surface to suc-

cessfully prevent oxidation. However, due to the brittle and hard nature of those inorganic films, cracking in the chip might not be reduced, and bond quality is reduced due to the amount of nonmetallic material at the interface.

Tin has been a common base material for soldering technology in the past decades. Tin plating has been used within a number of PCB manufacturing facilities as a final solderable metal finish, for both aesthetic purposes and a reliable Pb-free alternative. Tin plating has recently gained certain popularity in chemical processing due to the Pb-free finishes and lack of stripping residues. Because of the advantage of Sn PCB finishing for fine pitch and Pb-free applications, the move to adapt Sn as PCB finishing material in soldering technology has been made by many industrial users. Furthermore, it is known from Ray et al.⁶ that Sn is very effective to prevent materials from oxidation. They reported that a thin ($\sim 40 \text{ \AA}$) layer of SnO_x was observed on freshly deposited Sn, and after 6 days exposure at 65°C and 85% RH, the layer thickness grew only to 400 Å. Because Sn plating has a number of benefits in electronic packaging, this paper focuses on the application of Sn as a plating for wire bonding.

(Received November 9, 2006; accepted December 13, 2006; published online May 15, 2007)

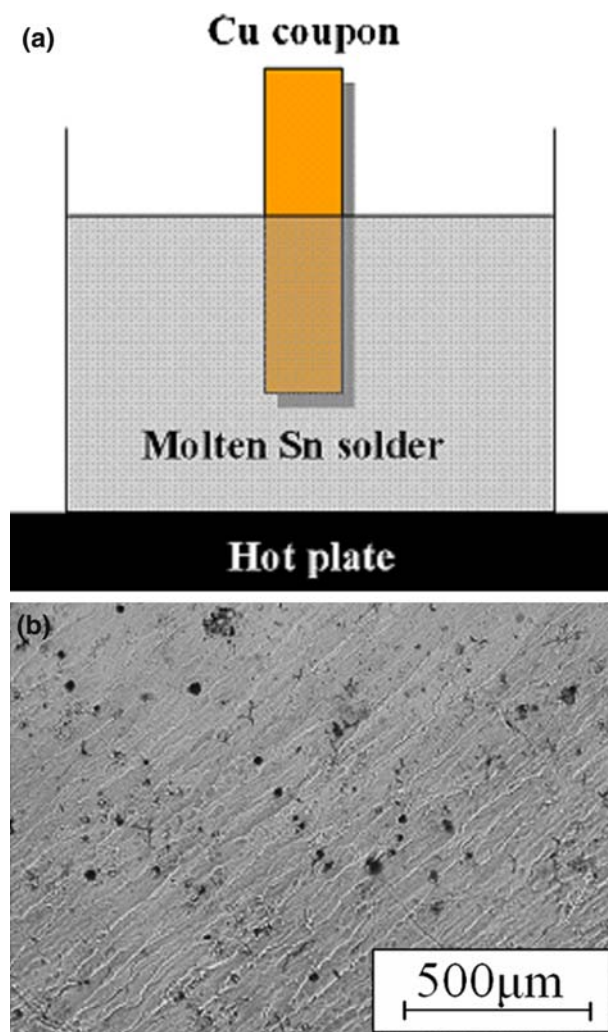


Fig. 1. (a) Sketch of dipping process used for Sn plating on Cu and (b) optical microscope image of sample 2 surfaces.

EXPERIMENTAL PROCEDURE

A hot plate at 250°C was used to liquefy 99.8% pure Sn. The 99.99% pure Cu coupons are 1 cm × 2 cm in size and 700 μm in thickness. Their main surfaces were ground with 1,200 and 2,400 digit SiC papers, washed first with acetone and then with 10% HCl, acetone, ethanol, and finally fluxed with liquid flux. To activate the flux, the Cu coupons were heated by placing them above the Sn bath for 1 minute before they were dipped in the solder bath. Dipping times used were 1 s and 30 s to produce samples 1 and 2, respectively. Figures 1a and b show a sketch of the dipping process and the surface morphology of sample 2, respectively.

Continuous Sn layers are obtained on both samples. Micro x-ray diffraction (μ -XRD) was performed with a Rigaku (Tokyo, Japan) AFC-SC + SAT 70 μ -XRD to identify the phases in the layers. Accelerating voltage and current used were 50 kV and 40 mA, respectively. To measure the thicknesses of

the Sn layers, the samples were cross sectioned with a diamond saw, ground with 1,200 and 2,400 digit SiC papers, and then polished in several steps with 1- μ m, 0.3- μ m, and 0.04- μ m Al₂O₃ powders.

A 25- μ m-diameter AW8 Au wire manufactured by American Fine Wire (Subsidiary of K&S, Willow Grove, PA) was used to bond wires on samples 1 and 2. The capillary used was a Kulicke & Soffa (K&S, Willow Grove, PA) (part no. 40472-0012-334) with hole and chamfer diameters of 42.5 μ m and 80 μ m, respectively. The Au ball bonding was performed using a Kulicke & Soffa 4524D semiautomatic ball bonder with 60-kHz ultrasonic frequency in the ball bumping mode with process temperatures of 150°C. Ten bonds at each condition were made. Bonding forces were set to 30 gf, 40 gf, 50 gf, and 80 gf. The ultrasonic powers were 390 mW, 520 mW, 650 mW, and 780 mW. The bonding time was 50 ms. The free air ball diameter was 57 μ m.

After wire bonding, all bonds were sheared with a DAGE 4000 (Dage precision industries, Inc., Fremont, CA, USA) shear tester. Shear speed and shear tip height were set to 100 μ m/s and 5 μ m, respectively. Cross sections of the ball-bonded samples were produced with a low speed diamond saw, ground with 1,200 and 2,400 digit SiC papers, and then polished with 1- μ m diamond paste. Microstructures and fracture surfaces were analyzed with a scanning electron microscope (SEM) using secondary electron (SE) and backscattered electron (BSE) microscopy equipped with energy-dispersive x-ray spectroscopy (EDX).

RESULTS AND DISCUSSION

Characteristics of Sn-Plated Cu

Figure 2a and b show BSE and EDX images of the cross section of sample 1, respectively. The EDX mapping, as shown in Fig. 2b, was used to visualize the Sn contents and location in the sample. The layer thickness was measured at 20 locations using the SEM, and the average value was determined. The average experimental thicknesses \pm standard deviations of the Sn layers on samples 1 and 2 are $0.85 \pm 0.08 \mu$ m and $5.34 \pm 0.21 \mu$ m, respectively. On sample 2, pores were observed in the Sn layer, and intermetallic compounds (IMCs) exist between the Sn layer and the Cu coupon with a thickness of about 1 μ m, as shown in Fig. 2c.

To identify the phases of the layers, an XRD analysis was performed on the surface of sample 1 by scanning with an 0.8-mm x-ray collimator over a 2θ range of 20–90° at 0.02°/s using Cu K_α radiation. The XRD result shown in Fig. 3 indicates that Cu and Sn elements are the most constituent material of the Sn-plated Cu. The peaks associated with Cu-Sn IMCs are Cu₆Sn₅ peaks. The intensity of the Cu₆Sn₅ peak is much weaker than that of the Sn layer and the Cu bulk. It is concluded that the Cu₆Sn₅ layer is much thinner than the Sn layer. Even though the Cu₆Sn₅ peaks are weak, they are

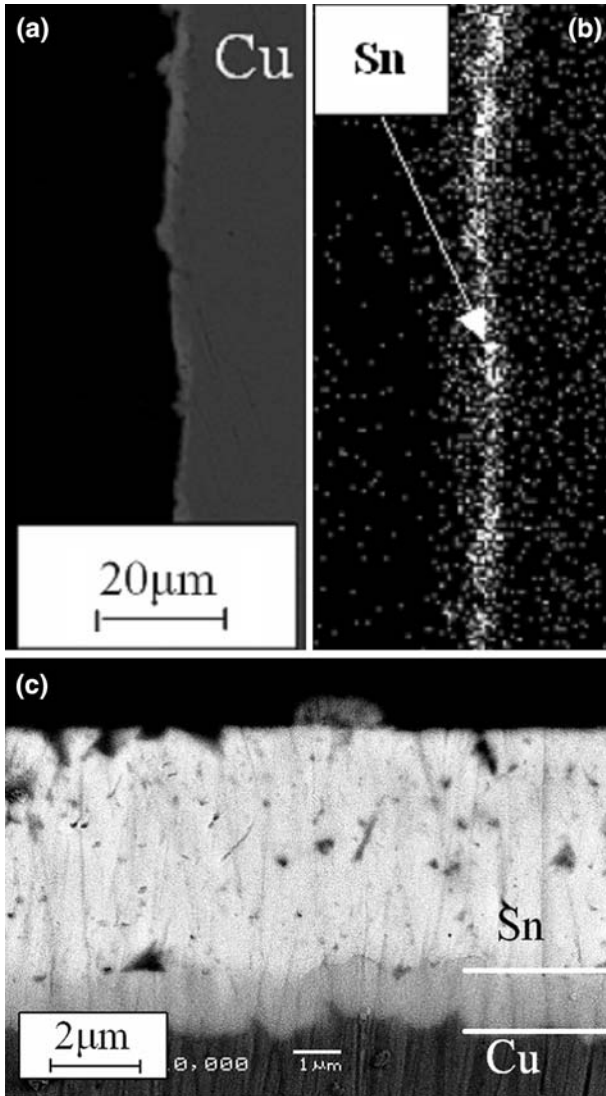


Fig. 2. Cross-sectional images of Sn-plated Cu coupons: (a) BSE image of sample 1; (b) EDX mapping of Sn, same location as image (a); and (c) BSE image of sample 2.

significant and indicate the presence of Cu_6Sn_5 even in sample 1.

Microstructure Observed at the Interface of Ball Bonds on Sn-Plated Cu

As seen in Fig. 4a, the Au ball was successfully bonded on sample 1. Figure 4b shows the enlarged version of the square in Fig. 4a. No defects at the interface were found in Fig. 4a and b. Two layers, denoted "A" and "B," were formed between the ball and the substrate, as defined in Fig. 4b. The average thicknesses of both layers is $0.5 \mu\text{m}$. The thicknesses vary to more than $1 \mu\text{m}$.

The EDX results shown in Table I from the regions with thicknesses of the layer more than $1 \mu\text{m}$ indicate that both layers are composed of Au, Cu, and Sn elements. The A layer is composed of

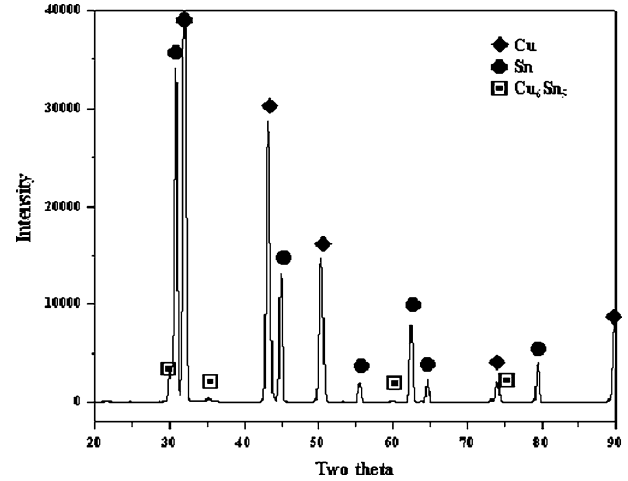


Fig. 3. XRD pattern of sample 1.

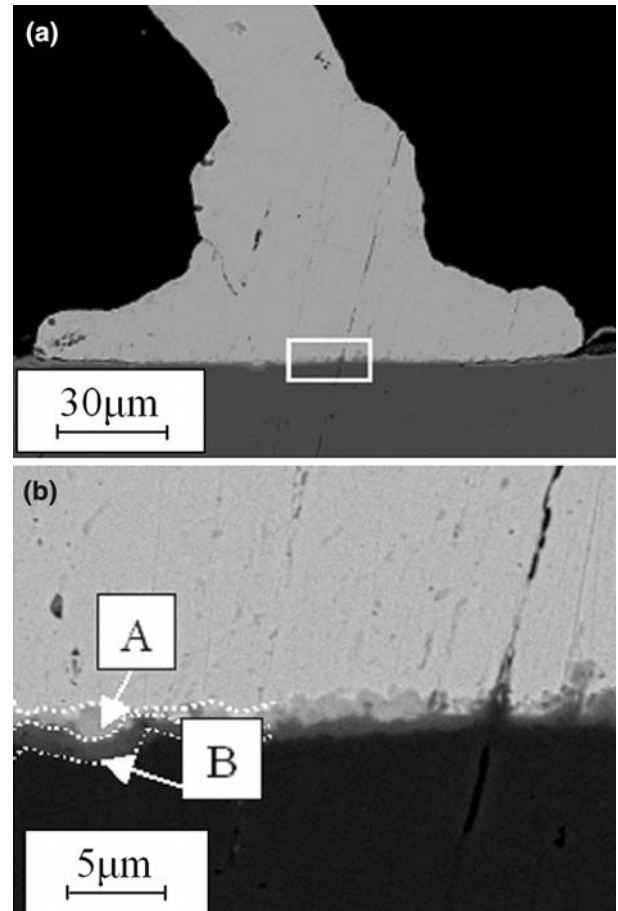


Fig. 4. BSE images showing (a) ball bond after wire bonding on sample 1 (150°C , 80 gf, and 520 mN) and (b) enlarged image of the square in (a).

62wt.%Au, 33wt.%Sn, and 5wt.%Cu. The B layer consists of 53wt.%Sn, 41wt.%Cu, and 6wt.%Au.

Ball bonds were successfully made on sample 2. An example cross section is shown in Fig. 5. A large amount of expelled material (flashes) is observed

Table I. Compositions of A and B Layers by EDX

Layers	Au (Wt/At.%)	Cu (Wt/At.%)	Sn (Wt/At.%)	Possible Phases
A	62/46	5/12	33/41	$(\text{Au,Cu})\text{Sn}^7$
B	6/3	41/58	53/39	$(\text{AuCu})_6\text{Sn}_5^8$

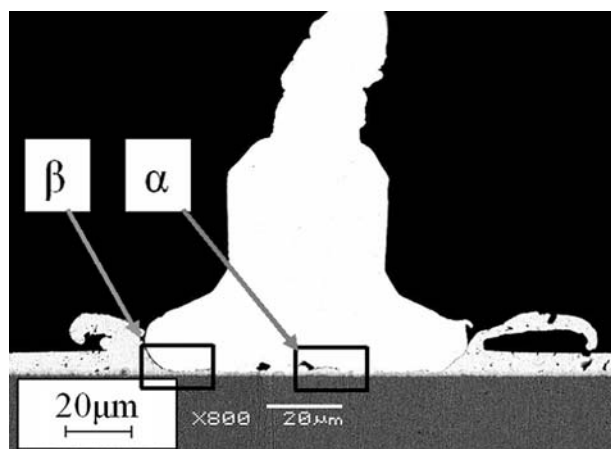


Fig. 5. BSE image of ball bonded on sample 2. Temperature, bonding force, and ultrasonic power were 150°C, 80 gf, and 520 mN, respectively. Details of α and β squares are shown in Fig. 7.

next to the edge of the ball bond contact zone. The flashes mainly consist of Sn. The flashes are about 25 μm in length in the ultrasonic direction. They are smaller perpendicular to the ultrasonic direction. It appears that ultrasonic vibration produces these flashes because they were mainly found in the ultrasonic direction. An EDX analysis was performed on the flashes formed on the edge of the ball bond, as shown in Fig. 6a and b. The result shows that the flashes are Sn, indicating the squeezing out of Sn by ultrasonic action. Similar but smaller flashes usually are observed in Au-Al and Cu-Al wire bonding. The flashes are produced by pad material plasticized by the combination of normal and ultrasonic stresses and transported to the contact zone periphery by the shear stresses during the bonding process.

The interface observation in Fig. 7a shows that three layers (C, D, and E) were formed during wire bonding. The combined thickness of the C and D layer is about 1.5 μm . The E layer thickness is approximately 1.3 μm . Very small voids are observed in the C layer as well as on the interface between the Au ball and C layer. A dark gray layer E is observed close to the Cu coupon. The observation of the periphery of the ball bond in Fig. 7b shows small cracks between the Au ball and Cu-Sn IMCs. It appears that the C layer does not exist at the periphery.

The EDX results in Table II show that the three layers C, D, and E are composed of Au, Sn, and Cu elements. The amounts of Sn in the layers C, D, and

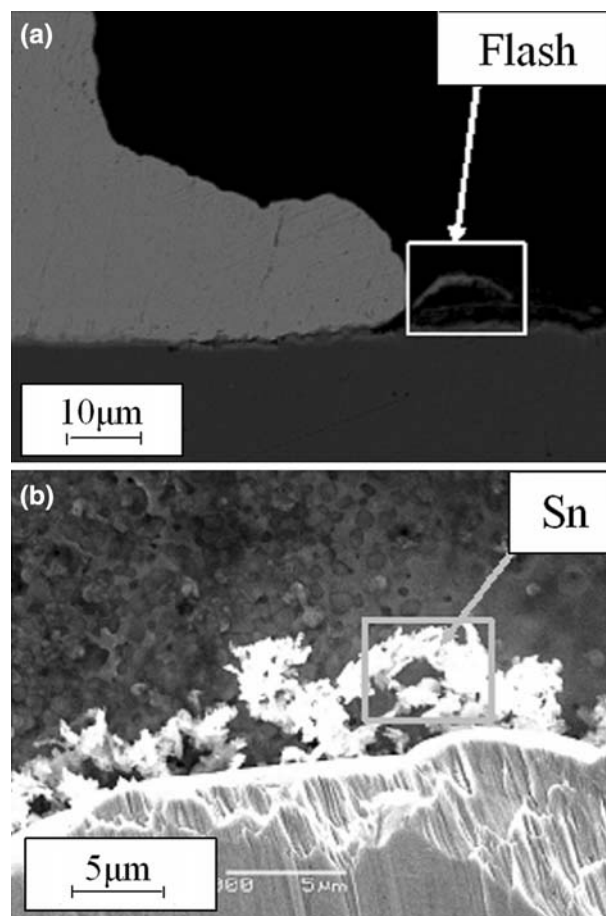


Fig. 6. SEM images showing Sn flash indicated by arrows after wire bonding on sample 1 (150°C, 80 gf, and 520 mN): (a) cross-sectional view and (b) top view after shear test.

E are in the range of 40–44 at.%, whereas the amount of Au significantly varies from 43 at.% to 11 at.% and the amount of Cu from 13 at.% to 49 at.%. However, the sums of the Au and Cu amounts show no significant difference in C, D, and E. Because the Au-Cu system¹³ has continuous solid solubility characteristics for all compositions, Au and Cu atoms can replace each other without forming intermetallic phases. The Au-Cu system is known to experience ordered transformation below 390°C, which means that the Au atoms preferentially occupy corner positions in the unit cell, giving a simple cubic lattice, and the Cu atoms preferentially occupy the face-centered positions.¹⁴ Hence, this transformation results in a substitutional solid solution.

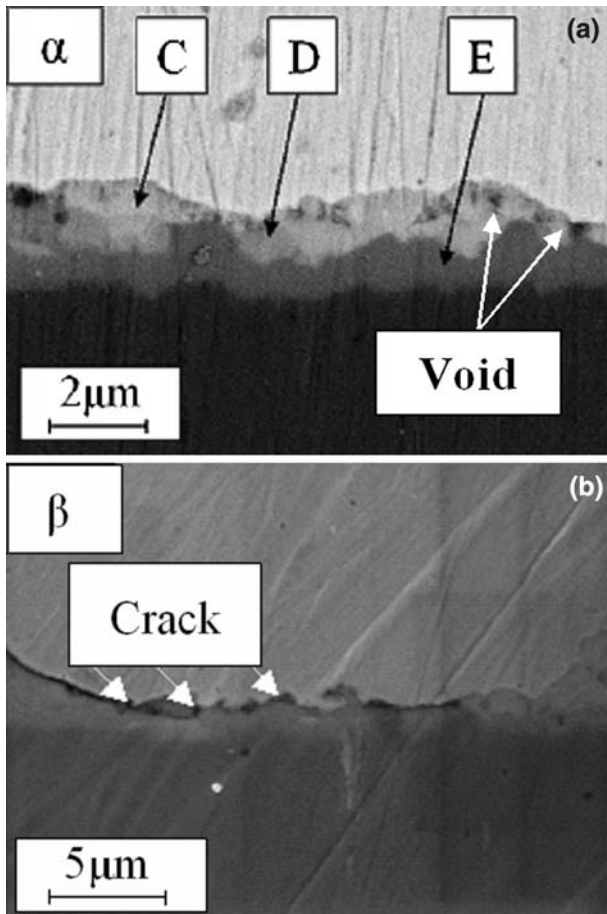


Fig. 7. Microstructure of ball bonded on sample 2. (a) and (b) Square α and β in Fig. 5, respectively.

Table II. Compositions of C, D, and E Layers by EDX

Layer	Au (Wt/At.%)	Cu (Wt/At.%)	Sn (Wt/At.%)	Possible Phases
C	59/43	6/13	35/44	(Au,Cu)Sn
D	44/28	14/28	42/44	(Au,Cu) ₆ Sn ₅
E	22/11	30/49	48/40	(Au,Cu) ₆ Sn ₅ or Cu ₆ Sn ₅

The composition of the D layer consists of 28at.%Au, 28at.%Cu, and 44at.%Sn. Layer B is formed during dipping the Cu coupon into the Sn molten solder. The Cu₆Sn₅ layer is first formed as indicated by the XRD result shown in Fig. 3. During the bonding process, Cu atoms are replaced by Au atoms. The final phase of (Au,Cu)₆Sn₅ is formed.

Mechanical Strength of Ball Bonds and Fracture Surface Analysis

Shear tests were carried out to determine the mechanical strength of the Au ball bonds on the Sn-plated Cu of sample 1. Ball bonds on sample 2 were not tested because the large flashes at the edge

of ball bond make it impractical to measure the shear force of the ball bond alone.

Figure 8 shows the shear forces of balls bonded on sample 1 with bonding forces of 30 gf, 40 gf, 50 gf, and 80 gf and ultrasonic powers of 390 mW, 520 mW, 650 mW, and 780 mW. Each data point represents the average of ten shear tests and the error bars represent error, ε , which is calculated using

$$\varepsilon = \sigma / (n - 1)^{1/2} \quad (5)$$

where σ is the standard deviation, and n is the number of shear tests performed.

At an ultrasonic power of 390 mW, the effect of bonding force is dominant on shear force. However, as ultrasonic power is increased, the effect of bonding force decreases, which is consistent with a theoretical process prediction.¹⁵ As ultrasonic power increases from 390 mW to 520 mW the shear force increases. Above 520 mW of ultrasonic power, the shear force decreases for all used bonding forces. The highest shear strength, as defined by shear force divided by contact zone area (3,771 μm^2), was 100 MPa and was obtained with 520 mW and 40 gf of ultrasonic power and bonding force, respectively.

The results of the shear force measurement are in agreement with the microstructure of bonds made with 390 mW and 520 mW, as shown in Fig. 9a and b. Only localized bonding is observed between the Sn and the Au ball in Fig. 9a, indicating poor bonding with 390 mW, which is shown by the low shear force. With 520 mW, a large bonded interface between Au wire and Cu substrate is observed, resulting in high shear force, as shown in Fig. 9b.

Figure 10a–d show the fracture surfaces obtained after shearing balls bonded with 40 gf of bonding force and various ultrasonic powers. Fracture occurs mostly at the interface between Sn and gold ball for balls bonded with low ultrasonic power. Only a small amount of Au is observed at the fracture surface shown in Fig. 10a. Fracture occurs in the Au ball bonded with 520 mW, as shown in Fig. 10b, indicating strong bonding. However, when

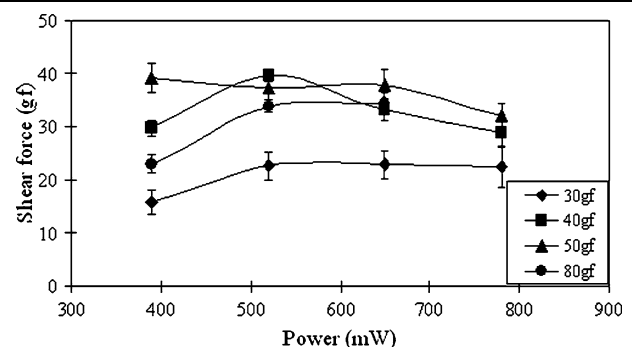


Fig. 8. Shear force versus powers of balls bonded on sample 1.

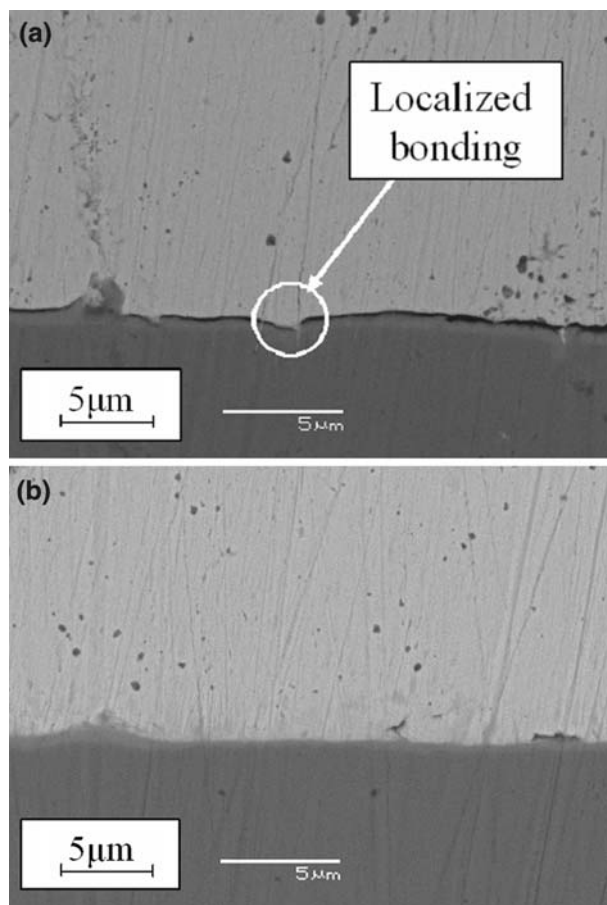


Fig. 9. BSE images showing microstructures of cross sections of ball bonded on sample 1 with (a) 390°C and (b) 520°C. Bonding force, temperature, and time were 40 gf, 150°C, and 50 ms, respectively.

bonded with 650 mW and 780 mW, as shown in Fig. 10c and d, respectively, the Au balls excessively deform, resulting in ball height lower than 5 μm . Shearing occurred in the ball neck region, resulting in shear force readings that cannot be compared with those of bonds with normal deformation.

The shear fracture of another ball bonded with 390 mW and 40 gf bond force did not occur in the gold ball but at the bond interface. The fracture surface is studied in greater detail using Fig. 11a–c. It can be seen that fracture occurred not only between Sn and Au, but also between the IMC and Sn layers. The IMCs are exposed after shear test, as shown in Fig. 11b. The EDX results suggest that the IMCs are Cu_6Sn_5 . White particles indicating gold debris are observed on the IMCs and Sn layer, as shown in Fig. 11b and c, respectively.

Interface Temperature

Earlier studies were performed to understand the nature of adhesion and how it is achieved in the ultrasonic wire bonding process.^{16,17} The studies tried to find an answer to the question of whether melting occurred on the interface of two metals during ultrasonic wire bonding. They concluded that ultrasonic wire bonding is a solid-state process, i.e., no melting occurs.

The present work reinvestigates the possibility of Sn melting during the bonding process. A bonding test is performed with a largely increased force and ultrasonic parameters. Schneuwly et al.¹⁸ reported that in their test the ball temperature rose to 120°C at 2 N, 2 W, and 20 ms of applied force, ultrasonic power, and a time, respectively. Joshi¹⁹ reported the

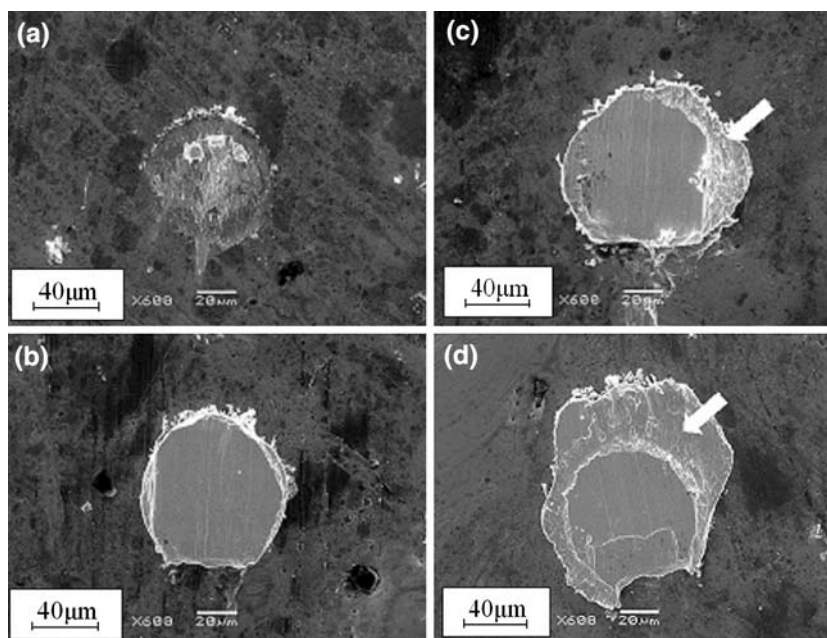


Fig. 10. Fracture surface images after shear test of ball bonded with (a) 390°C, (b) 520°C, (c) 650°C, and (d) 780°C. Bond force and temperature were 40 gf and 150°C, respectively.

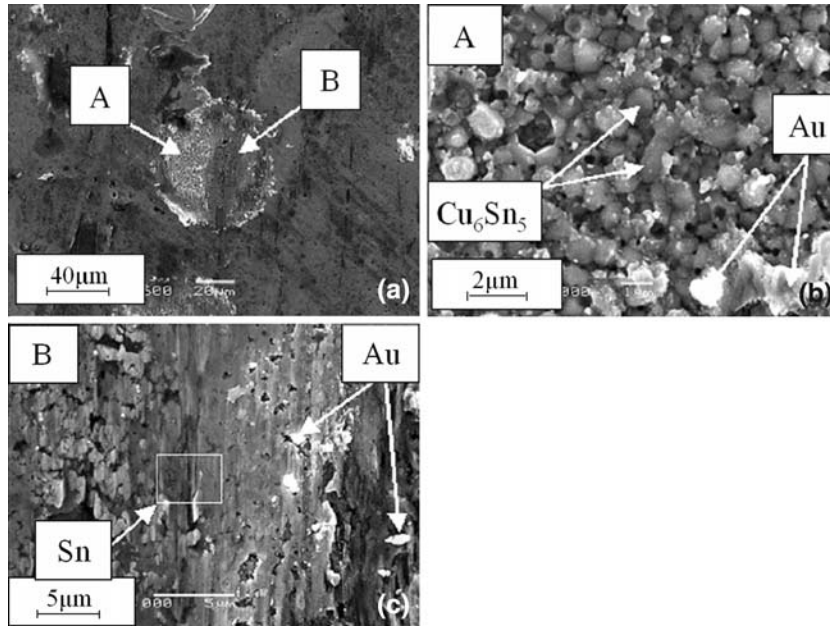


Fig. 11. (a) Fracture surfaces of a second sample obtained with 40 gf, 390°C, and 150°C. (b) and (c) Enlarged images taken at points “A” and “B” of (a), respectively.

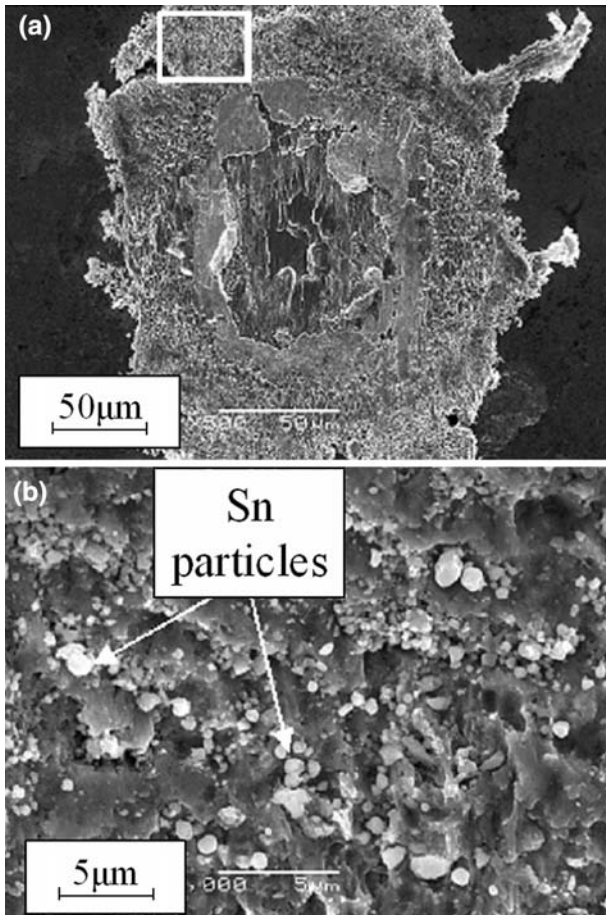


Fig. 12. SEM images showing (a) fracture surface after wire bonding on sample 2 and (b) enlarged image of square in (a) (80°C, 80 gf, and 910 mN).

temperature rise of up to 80°C at the interface during the bonding. In this study, the wire bonding was performed at 150°C. The eutectic temperature, 217°C, of Au and Sn could be reached if a portion of the interface is heated by at least 67°C during the bonding test. If similar temperature rises as reported in (References 18 and 19) were produced, the temperature during wire bonding could rise high enough to cause melting of Sn.

Figure 12a and b show the fracture surface observed on sample 2 after shearing a ball bonded with 80 gf and 910 mW, each of these parameters being approximately double the optimized values. The ultrasonic direction was from top to bottom. Flash is observed outside the fracture surface and is longest along the ultrasonic direction. Figure 12b is an enlarged image of the square in Fig. 11a and shows circular Sn particles that possibly are solidified droplets formed due to the surface tension of liquid Sn. The circular Sn particles suggest that melting has occurred during the bonding test.

CONCLUSIONS

- Uniform thicknesses of Sn layers are observed if they are produced by dipping a Cu sample into molten Sn for 1 s and 30 s, respectively. On the Cu sample, a Cu_6Sn_5 layer coexists with Cu and Sn after dipping. After 30 s dipping, the Cu_6Sn_5 thickness is 1.5 μm .
- The feasibility of gold wire bonding on Sn metalizations is confirmed in this study. At the bonded-on sample dipped for 1 s, balls with the highest

shear strength of 100 MPa are bonded with 520°C and 40 gf of ultrasonic power and bonding force, respectively.

- At the interface of a Au ball bonded on samples dipped for 30 s, Sn mainly exists in the center of the ball bond and the thickness of the Au-Sn layer is larger than that observed with the 1-s dipping sample.
- During wire bonding on Sn-plated Cu, Sn is partly squeezed out of the contact zone. This flash extends about 10 μm for the thin metallization and up to 25 μm for the thick metallization.
- Circular Sn particles that possibly are solidified droplets are found at the fracture surface of bonds made with increased ultrasonic power and bonding force. This indicates that melting of Sn has possibly occurred during the modified process. No such indication is observed with the optimized process.

REFERENCES

1. G. Harman, *Wire Bonding in Microelectronics: Materials, Processes, Reliability, and Yield* 2nd ed, (New York: McGraw-Hill, 1997).
2. M. Miyamoto, T. Takeda, and T. Furusawa, *IEEE Trans. Electron. Dev.* 44, 250 (1997).
3. J.N. Aoh and C.L. Chuang, *J. Electron. Mater.* 33, 290 (2004).
4. M. Sivakumar, V. Kripesh, C.S. Choong, C.T. Chon, and L.A. Lim, *Microelectron. Reliab.* 42, 1535 (2002).
5. G. Harman and C.E. Johnson, *IEEE Trans. Comp. Packag. Technol.* 25, 677 (2002).
6. U. Ray, I. Artaki, and H.M. Gordon, *J. Electron. Mater.* 23, 779 (1994).
7. H. Okamoto and T.B. Massalski, *Binary Alloy Phase Diagrams* 2nd ed, (Materials Park, OH: ASM International, 1990).
8. N. Saunders and A.P. Miodownik, *Binary Alloy Phase Diagrams* 2nd ed, (Materials Park, OH: ASM International, 1990).
9. R.A. Gagliano and M.E. Fine, *J. Electron. Mater.* 32, 1441 (2003).
10. Y.C. Chan, A.C.K. So, and J.K.L. Lai, *Mater. Sci. Eng.* B55, 5 (1998).
11. A. Hayashi, C.R. Kao, and Y.A. Chang, *Scripta Mater.* 37, 393 (1997).
12. K.L. Erickson, P.L. Hopkins, and P.T. Vianco, *J. Electron. Mater.* 23, 729 (1994).
13. H. Okamoto, K.J. Chakrabarti, D.E. Laughlin, and T.B. Massalski, *Binary Alloy Phase Diagrams* 2nd ed, (Materials Park, OH: ASM International, 1990).
14. B.D. Cullity, *Elements of X-Ray Diffraction* 2nd ed, (CA: Addison-Wesley, 1978).
15. M. Mayer and J. Schiwizer, *Proc. 5th Electronic Packaging Technology Conf.* (Singapore: IEEE/EPTC, 2003), pp. 738–743.
16. J.E. Krazanowski and N. Murdeshwar, *J. Electron. Mater.* 19, 919 (1990).
17. G. Harman and J. Alberts, *IEEE Trans. Parts, Hybrids Packag.* PHP-13, 406 (1977).
18. A. Schnewly, P. Groning, L. Schlapbach, and G. Muller, *J. Electron. Mater.* 27, 1254 (1998).
19. K.C. Joshi, *Weld. J.* 50, 840 (1971).